Macromolecules

ARTICLE

pubs.acs.org/Macromolecules

Heat Capacity of Spider Silk-Like Block Copolymers

Wenwen Huang,[†] Sreevidhya Krishnaji,[‡,§] Xiao Hu,[§] David Kaplan,[§] and Peggy Cebe[†,*]

[†]Department of Physics and Astronomy, Tufts University, Medford, Massachusetts 02155, United States

[‡]Department of Chemistry, Tufts University, Medford, Massachusetts 02155, United States

[§]Department of Biomedical Engineering, Tufts University, Medford, Massachusetts 02155, United States

ABSTRACT: We synthesized and characterized a new family of diblock copolymers based on the amino acid sequences of *Nephila clavipes* major ampulate dragline spider silk, having the form HAB_n and HBA_n ($n = 1-3$), comprising an alanine-rich hydrophobic block, A, a glycine-rich hydrophilic block, B, and a histidine tag, H. The reversing heat capacities, $C_p(T)$, for temperatures below and above the glass transition, T_g, were measured by temperature modulated differential scanning calorimetry. For the solid state, we then calculated the heat capacities of our novel block copolymers based on the vibrational motions of the constituent poly(amino acid)s, whose heat capacities are known or can be estimated from the ATHAS Data Bank. For the liquid state, the heat capacity was estimated by using the rotational and translational motions in the polymer chain. Excellent agreement was found between the measured and calculated values of the heat capacity, showing that this method can serve as a standard by which to assess the C_p for other biologically inspired block copolymers. The fraction of β sheet crystallinity of spider silk block copolymers was also determined by using the predicted C_p, and was verified by wide-angle X-ray diffraction and Fourier transform infrared spectroscopy. The glass transition temperatures of spider silk block copolymer were fitted by Kwei's equation and the results indicate that attractive interaction exists between the A-block and the B-block.

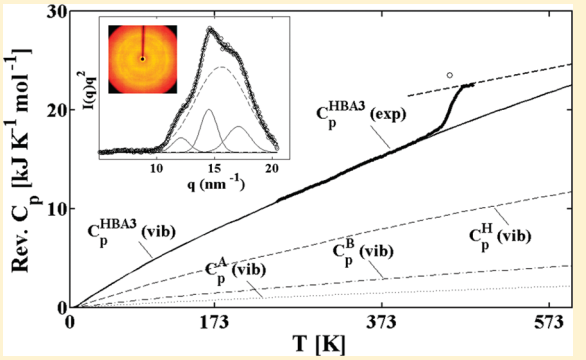

1. INTRODUCTION

Silks are generally defined as externally spun fibrous protein secretions produced by some lepidoptera larvae such as silkworms, spiders, scorpions, and mites. Spider silks are synthesized in glands located in the abdomen and spun out through a series of spinnerets of spiders.[1] These fibers are remarkable materials when considering their light density, excellent mechanical properties, and thermal stability over a wide range of temperature. On a strength-to-weight basis, the average ultimate tensile strength and elongation at break of spider silks are the same as, or even higher than, Kevlar and steel.[2−4] Spider dragline silk is thermally stable to about 230 °C according to thermogravimetric analysis (TGA).[5] Because of these attractive properties, spider silks have received extensive research attention. Spider silks differ in properties, composition, morphologies and functions depending on their primary amino acid sequences and the type of silk gland through which they are spun. For example, the spider dragline silk from the major ampullate gland is for orb web frame and radii construction; the spider viscid silk from the flagelliform gland is for prey capture; the spider wrapping silk from the aciniform gland is for wrapping captured prey; and the spider glue-like silk from the aggregate gland is for attachment.[6] Among over 30,000 species of spiders (class *Arachnida*),[7] the orb-weaving spider, *Nephila clavipes*, has become the most well understood with its dragline silk the best characterized.

Spider silk is also a good example of a natural block copolymer, in which alanine-rich hydrophobic blocks and glycine-rich hydrophilic blocks are linked together generating a functional polymer used in biomedical applications such as guided tissue repair and drug delivery.[8,9] The spider dragline silk of *N. clavipes* from the major ampullate gland contains at least two different proteins, major ampullate dragline silk protein 1 (MaSp1) and major ampullate dragline silk protein 2 (MaSp2), which are held together by three to five disulfide bonds.[10] The main difference between MaSp1 and MaSp2 is that MaSp1 is a proline free protein, while the total amino acid content of MaSp2 contains 15% proline residues, which is known as a strong β-sheet breaker due to its unique pyrrolidine ring structure and the lack of one potential H-bond donor.[12−14] Biophysical studies have found evidence that different motifs are responsible to form various secondary structures corresponding to silk's mechanical properties. The GA/A_n motif forms β sheets structures that correspond to the crystalline regions in the spun fibers, which provide the high tensile strengths and stiffness;[6,11,15] the GG*X* motif forms α helices that give rise to a nonstructured amorphous region[10,16] to stabilize the fiber; and GPGG*X* motif have been hypothesized to form stackable type II β turns structures, which provide the elasticity and extensibility of the threads.[17]

Received: March 11, 2011
Revised: May 11, 2011
Published: June 16, 2011

Figure 1. Amino acid sequences: (a) A-block, B-block, and His-tag; (b) their copolymers, exemplified by HAB_3.

To provide further insight into the relationships among peptide amino acid sequence, block length, and structural features, we have embarked on a program to create synthetic proteins inspired by the genetic sequences found in spider dragline silks, and used these bioengineered spider silk block copolymers to study secondary structures and morphological features. In our present work, we have chosen as a model system, diblock copolymers based on MaSp1 motifs, GA/A_n and GGX, and mass produced a family of diblock copolymers, which possess these motifs as their blocks, using recombinant DNA technology. Because of the hydrophobic and hydrophilic nature of the blocks, the spider silk block copolymers tend to self–assemble to form periodic nanostructures.[18,19]

Thermal property studies of these copolymers are also very crucial. To obtain a fuller understanding of these novel materials, in our work, we use a model to calculate the heat capacity of spider silk block copolymer in the solid or liquid state, below or above the glass transition temperature, respectively. We characterize the thermal phase transitions and other thermal properties by temperature modulated differential scanning calorimetry (TMDSC) and thermogravimetric analysis (TGA). We also assess the crystal structure and secondary structure by Fourier transform infrared spectroscopy (FTIR) and wide-angle X-ray diffraction (WAXD). The methods used here can serve as a standard way to assess the structural features and crystallinity of biological diblock copolymers. Aside from the fundamental perspective, we also anticipate that these results will provide a roadmap for the design and synthesis of precise materials having some of the same properties of spider silks, or other valuable rare material, using well controlled protein sequences.

2. EXPERIMENTAL SECTION

2.1. Materials. Two spider silk amino acid sequences were picked as the blocks, named A-block (hydrophobic) and B-block (hydrophilic), respectively (Figure 1a). A-block and B-block polypeptides were purchased from Tufts Protein Synthesis Laboratory in powder form, and then purified. The diblock copolymers containing a His-tag H were biosynthesized in our laboratories. The synthesis method of these block copolymers was described in our previous paper.[18] In brief, after constructing cloning vector, cloning silk modules into a pET30L vector, expressing and purifying spider silk block copolymers, biosynthesized block copolymers with His-tag H, HAB_3, HBA, HBA_2, and HBA_3 (Figure 1b), were obtained in solid form. Protein identification was confirmed by matrix assisted laser desorption ionization mass spectrometry (MALDI−TOF; Chemistry Department, Tufts University, Medford, MA). Calculated and measured molecular weights are summarized in Table 1.

Table 1. Molecular Weight of Spider Silk Block Copolymers

sample	calculated M_w (Da)	measured M_w (Da)
B	1938	1938
HAB_3	11 967	11 965
HBA	8127	8137
HBA_2	9097	9095
HBA_3	10 068	10 057
A	989	989

The spider silk block copolymers were dissolved into water at a concentration of 2 mg/mL, and cast into films about 10 μm thick on a calcium fluoride (CaF_2) substrate for FTIR. Free standing films about 300 μm thick were also cast from the same solution on Teflon substrate for DSC, TGA, and WAXD. Films were placed into a vacuum oven at 25 °C for 24 h to remove the surface water.

2.2. Thermal Analysis. *Temperature Modulated Differential Scanning Calorimetry (TMDSC).* Samples with mass about 2 or 3 mg were encapsulated into aluminum pans and heated in a TA Instruments Q100 DSC, which was purged with dry nitrogen gas at a flow rate of 50 mL/min. The temperature and heat flow of the DSC were carefully calibrated using indium standard before experiments. The samples were annealed in the DSC at 120 °C for 60 min to eliminate the surface water absorbed during handling before each run. The total weight of pan and lid for sample encapsulation and reference were kept the same in all runs.

TMDSC was performed at a heating rate of 2 °C/min from −30 to +350 °C with an oscillation amplitude of 0.318 °C and a modulation period of 60 s. To measure the reversing heat capacity, we used a "three run method", as described in our earlier work.[20] The first run is empty aluminum sample pan versus empty aluminum reference pan to obtain the cell asymmetry and baseline correction. The second run is sapphire standard in aluminum pan versus empty aluminum reference pan to calibrate heat flow amplitude according to standard equations.[21,22] The third run is sample in aluminum pan versus empty aluminum reference pan. The same empty aluminum reference pan was used in all the runs, and all the aluminum sample pans were kept the same in weight.

The basic mechanism of quantitative TMDSC involves adding a sinusoidal temperature modulation to the conventional linear temperature ramp to separate reversing and nonreversing heat effects within the temperature range of the modulation. The time dependence of sample temperature is expressed as

$$T_s(t) = T_0 + qt + A_T \sin(\omega t - \varepsilon) \quad (1)$$

where T_0 is the initial temperature, q is the underlying linear heating rate, A_T is the corresponding modulation amplitude, ω is the modulation frequency, and ε is the phase shift with respect to the reference.

In TMDSC, the signal deconvolution is accomplished by a mathematical technique known as discrete fourier transformation (DFT).[23] As the first step in the deconvolution process, the raw data are averaged over one complete period to remove the modulation. This gives the total heat

flow and the deconvoluted temperature, which is equivalent to information obtained by standard DSC. Then the averaged signal is subtracted from the raw data and DTF procedure is applied with a sliding transform window to obtain the amplitude and phase difference of the heat flow response at modulation frequency ω so as to obtain the reversing heat capacity.[24] The heat capacity in TMDSC can be expressed as:

$$|mc_p + C_s - C_r \pm \Delta C_{cell}| = \frac{A_\Delta}{A}\sqrt{\left(\frac{K}{\omega}\right)^2 + {C_r}^2} \quad (2a)$$

$$= \frac{A_{HF}}{A}K' \quad (2b)$$

where mc_p is the heat capacity of a sample of mass, m, and specific heat capacity, c_p; C_s and C_r are the heat capacities of the sample pan and empty reference pan, respectively; ΔC_{cell} is the cell asymmetry correction.[20] On the right-hand side of eq 2a, A_Δ is the amplitude of temperature difference between sample and reference; A is the sample temperature modulation amplitude; K is Newton's law calibration constant. In eq 2b, A_{HF} is the heat flow amplitude and K' is a calibration constant[25] related to the experimental conditions.

Using the sample specific heat capacity c_p, determined by the "three run method" and eq 2b, we obtain the reversing heat flow, RHF(t) as:

$$\mathrm{RHF}(t) = mc_p\left(\frac{\mathrm{d}T_s}{\mathrm{d}t}\right) \quad (3)$$

The non-reversing heat flow, NHF(t), is computed as the difference between the total heat flow, HF(t), and the reversing heat flow, RHF(t):

$$\mathrm{NHF}(t) = \mathrm{HF}(t) - \mathrm{RHF}(t) \quad (4)$$

Since thermodynamic equilibrium has not been assured during scanning, the term "reversing" is used rather than "reversible." The reversing heat flow refers to that component which is reversing within the time scale of the temperature oscillation. The glass transition phenomenon is an example of a transition which is reversing. Nonreversing processes include melting and crystallization, or degradation.

Thermogravimetric Analysis (TGA). Samples with masses about 4.0 mg or 5.0 mg were encapsulated in aluminum DSC pans to prevent powder sample from being blown out of the pan by nitrogen gas flow. Several holes ($d \sim 1$ mm) were made on DSC lids to let the sample surface be exposed to the atmosphere to let degradation products escape. Samples were heated in a TA Instruments Q500 thermogravimetic analyzer, which was purged with a dry nitrogen gas at a flow rate of 60 mL/min. Before each run, the empty pan was used to calibrate the zero point of the total weight. The experiments were performed at a heating rate of 2 °C/min from 25 to 400 °C.

2.3. Wide Angle X-ray Diffraction (WAXD). Water cast sample films about 300 μm in thickness were mounted in a Bruker GADDS D8 X-ray diffractometer (wavelength λ = 0.154 nm) operated at 40 kV and 20 mA. Scattering angle, 2θ, was calibrated by using silicon powder reference standard with silicon (111) peak at 28.444°. The scan time used was 1800s per sample. The scattering angle, 2θ, ranged from 4° to 28°. The air background was subtracted from the original scan for each sample. To compare the peak position and identify the crystalline content, the 2-D WAXS patterns were converted to a one-dimensional pattern by integrating with χ over all sectors (the beam stop region is avoided). The baseline was determined by subtracting air background and fitted using quadratic baseline. The crystallinity index, φ_{c_Xray}, was calculated using the ratio of the area of crystal peaks to the total scattered intensity by fitting the Lorentz-corrected WAXS peak intensity using Gaussian wave functions as described previously.[26,27]

2.4. Fourier Transform Infrared Spectroscopy (FTIR). Water cast sample film about 10 μm in thickness was cast onto CaF_2 substrate for FTIR measurements. Fourier transform infrared spectroscopy was carried out on a Jasco FT/IR-6200 with a TGS detector. The absorbance spectra were obtained by averaging 128 scans with a resolution of 4.0 cm^{-1}. The background spectra were collected under the same conditions and subtracted from the scan for each sample.

3. THEORETICAL BASIS

3.1. Calculation of Solid State Heat Capacity of Dry Block Copolymers. The heat capacity in the solid state of the genetically engineered spider silk block copolymers is determined based on the assumption that at sufficiently low temperature, the major part of the total heat capacity comes from vibrational motion. This common assumption has been successfully applied to calculate the heat capacity of synthetic polymers[28] as well as biopolymers, *Bombyx mori* silk fibroin,[29,30] from 0 K to the glass transition temperature.

The total solid vibrational heat capacity of dry spider silk block copolymer film, ${C_{p,vib}}^{Block\ copolymer}$, can be estimated as a linear combination of the vibrational heat capacities of each block through:[29]

$${C_{p,\,vib}}^{Block\,copolymer} = n_A {C_{p,\,vib}}^{Block\,A} + n_B {C_{p,\,vib}}^{Block\,B} + n_H {C_{p,\,vib}}^{Block\,H} \quad (5)$$

where ${C_{p,vib}}^{Block\ A}$, ${C_{p,vib}}^{Block\ B}$, and ${C_{p,vib}}^{Block\ H}$ are the solid vibrational heat capacity of each block, A, B and H; while n_A, n_B and n_H are the molar ratios of each block in the block copolymers. For example, in 1 mol block copolymer HBA_3, the molar ratios are $n_A = 3$, $n_B = 1$ and $n_H = 1$.

Following the method of Pyda et al.[29] the solid vibrational heat capacity of each block, ${C_{p,\,vib}}^{block\ I}$ (I = A, B or H), is constructed as a sum of products of the vibrational heat capacities of the individual poly(amino acid) residues, $C_p(i)$, by eq 6 using the Advanced Thermal Analysis System (ATHAS) data bank.[31]

$${C_{p,\,vib}}^{Block\,I} = N_{Ala}C_p(Ala) + N_{Gly}C_p(Gly) + N_{Ser}C_p(Ser) + \cdots + N_{Thr}C_p(Thr) = \sum_i N_i C_p(i) \quad (6)$$

where N_i is the total number of each kind of amino acid present in the amino acid sequence of an individual block. For example, in block A, $N_{Ala} = 7$, $N_{Gly} = 5$, *and* $N_{Ser} = N_{Thr} = 1$. Among 20 amino acids, the solid vibrational heat capacity data of 12 of them, alanine, asparagine, glycine, histidine, leucine, methionine, phenylalanine, proline, serine, tryptophan, tyrosine, and valine, are recorded in the ATHAS data bank. But for other amino acids, such as arginine, aspartic acid, cysteine, glutamic acid, glutamine, isoleucine, lysine, and threonine, the solid vibrational heat capacity data are not available in the ATHAS data bank. Therefore, we present a strategy[32] to estimate the unknown ones by the following method. (a) Because the side chain difference between threonine and serine is the same as the difference between alanine and glycine (Figure 2a), $C_p(Thr)$ can by estimated by using the solid vibrational heat capacities of other amino acids, which can be found in ATHAS data bank.[33] To estimate $C_p(Thr)$, we used: .

$$C_p(Thr) - C_p(Ser) = C_p(Ala) - C_p(Gly) \quad (7a)$$

For the same reason $C_p(Gln)$ can also be estimated by using $C_p(Asn)$, $C_p(Leu)$ and $C_p(Val)$ (Figure 2a). (b) For arginine, which has a relatively more complicated side chain, no amino acid with a similar structure can be found. But in the ATHAS data bank we find heat capacity data for poly(arginine) hydrogen chloride, poly(histidine) hydrogen chloride, and poly(histidine). Assuming the influence of HCl is the same for both

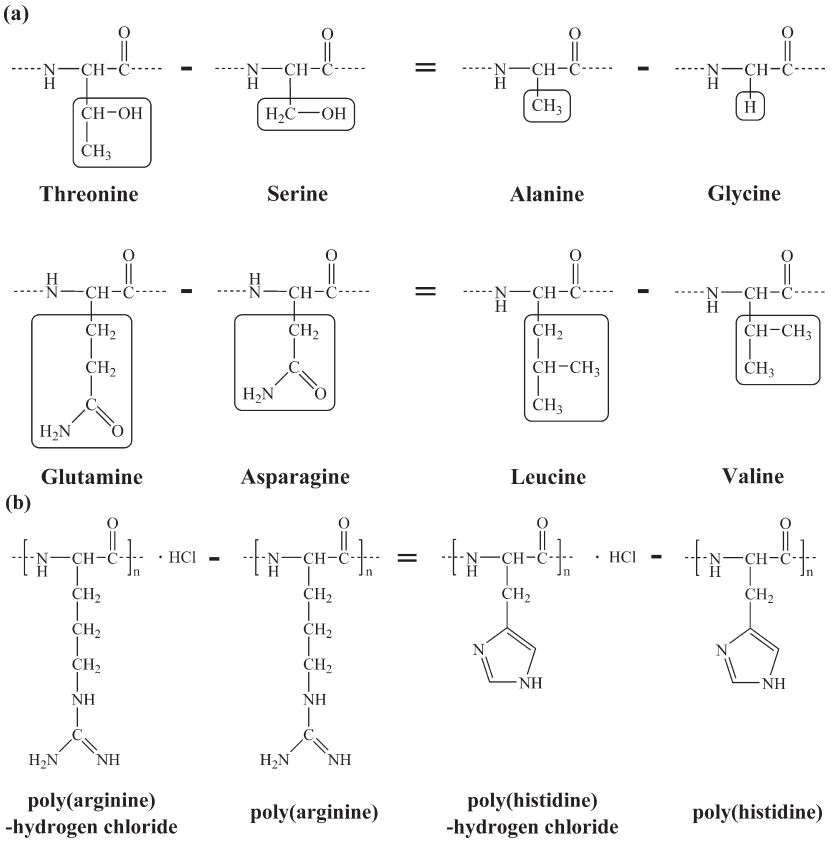

Figure 2. General scheme to estimate the vibrational heat capacity of an amino acid using an equation format for the chemical structure, illustrated by: (a) threonine and glutamine, with side chain of each amino acid highlighted by a rectangle, and (b) poly(arginine).

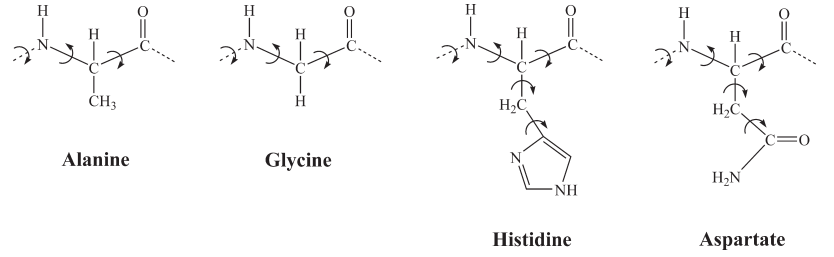

Figure 3. Mobile units in the poly amino acid residues, exemplified by alanine, glycine, histidine and aspartate. The arrows represent one rotational bond in each type of amino acid residue that changes the conformation of the chain at T_g. Alanine and glycine have three mobile units, while aspartate and histidine have five mobile units.

poly(arginine) and poly(histidine) (Figure 2b), we estimate $C_p(Arg)$ from:

$$C_p(Arg{-}HCl) - C_p(Arg) = C_p(His{-}HCl) - C_p(His) \quad (7b)$$

$C_p(Lys)$ can also be estimate by this method. The total solid vibrational heat capacity of spider silk block copolymers from the glass transition up to 1000 K were calculated using the strategy outlined above.

In TMDSC or DSC, the heating rates are not fast enough to prevent degradation of the biopolymers just above T_g. However, faster scanning rates are possible using thin-film (chip) calorimetry, which provides scanning rates as high as several thousand Kelvin per second.[34] For these fast scanning rates, the sample degradation could be deferred to a much higher temperature. Thus, extension of the calculated total solid vibrational heat capacity to temperatures above the TMDSC-determined glass transition could serve as a baseline for the fast heating techniques.

3.2. Calculation of Liquid State Heat Capacity of Dry Block Copolymers. The heat capacity in the liquid state (*i.e.*, viscous liquid, or rubbery state, of the polymer above T_g) is more complicated to estimate. Because the contribution comes not just from the vibirational motion, also the rotational and the translational degrees of freedom should be taken into consideration. According to Wunderlich,[35] each mobile unit in the polymer chain on average contributes 11 J/(mol K) to the change of heat capacity at the glass transition temperature, T_g. The number of mobile units of each kind of amino acid residue in

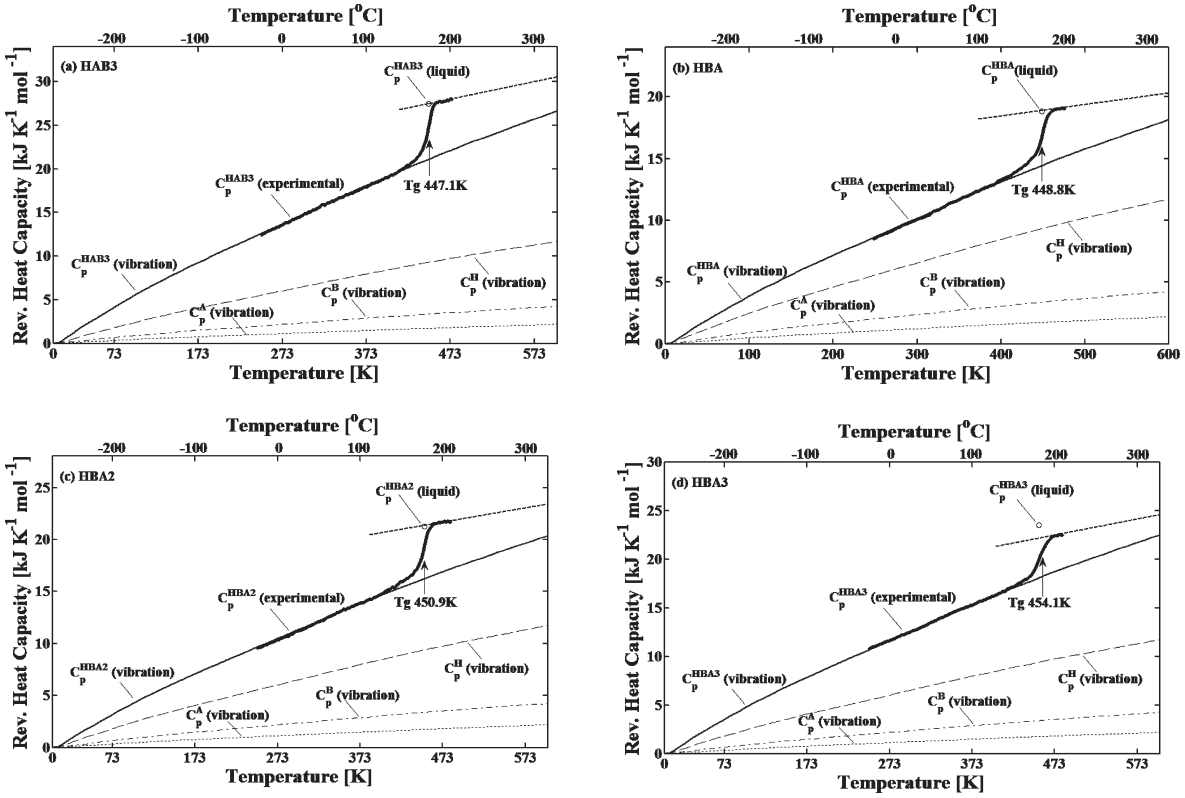

Figure 4. Experimentally measured and calculated apparent reversing heat capacity vs temperature, after annealing at 120 °C, for dry films of: (a) HAB_3, (b) HBA, (c) HBA_2, and (d) HBA_3. Key: heavy curve, $C_p(experimental)$; thin solid curve, $C_p(vibrational)$; open circles, $C_p(liquid)$ calculated at T_g. The individual solid state heat capacities of A-block (dotted curve), B-block (dash-dot curve), and His-tag (dashed curve) are shown for reference. Heavy dashed lines are extrapolated best fits to experimental curve above T_g.

our block copolymers can be determined from their chemical structure, shown in Figure 3.

By adding up the rotational bonds in the individual amino acid residues, the total number of mobile units that start to mobilize at T_g can be calculated. According to Pyda,[29] this rotational degree of freedom contributes approximately 91% of the heat capacity increment, ΔC_p, at the temperature T_g in dry *B. mori* silk fibroin. Though the sequence of the amino acid residues is different in a spider silk block copolymers, we assume this approximation should still be valid in our biomaterial, because genetically engineered spider silk block copolymers also consists of similar amino acid sequences to *B. mori* silk. Thus, the total degrees of freedom contributing to the change in heat capacity can be estimated as the sum of the contribution from each mobile unit divided by 91%. For example, there are 44 rotational bonds in one A-block, thus the heat capacity increment of A-block at the glass transition temperature is ΔC_p(A-block) = 44 × 11 J/(mol K)/91% = 537.8 J/(mol K).

4. RESULTS AND DISCUSSION

4.1. Modeling the Heat Capacity of Spider Silk Block Copolymer in the Solid and Liquid States. Determination of the heat capacity in the solid state of spider silk block copolymer from 0 K to the glass transition region is based on the assumption that contributions to the heat capacity come only from vibrational motions, $C_p(solid) = C_p(vibrational)$. It has been extensively studied that water in polymeric systems can affect the total heat capacity and the glass transition temperature.[30,36−38] To obtain the true glass transition temperature of dry spider silk block copolymers, we anneal the samples at 120 °C to eliminate the effect of bound water. During annealing, the water molecules escaped, and the total weight of sample changed. To avoid absorbing surface water from air again, we kept the sample in the DSC and estimate the sample weight after annealing by running the same experiment with TGA. After annealing, the spider silk block copolymers are free of bound water, and their true experimental reversing heat capacity was measured by TMDSC. Figure 4a−d shows a comparison of the calculated vibrational heat capacity (solid lines), $C_p(vibrational)$, with the experimental heat capacity (thick solid lines), $C_p(experimental)$, of spider silk block copolymers, HAB_3, HBA, HBA_2, and HBA_3, respectively. $C_p(experimental)$ was displayed only in the region (from −30 °C up to about +200 °C) for which region we are confident no degradation occurred in the samples. The vibrational heat capacity was constructed using the vibrational motion spectra of the individual amino acids (found in the ATHAS data bank[33] or estimated from the procedure of Figure 2) using eqs 5, 6 and 7, following the scheme discussed above.

The vibrational heat capacity of individual poly(amino acid)s in ATHAS were first calculated by Wunderlich and coworkers,[39,40] and developed by Pyda to apply them to the other biopolymers, such as *B. mori* silk fibroin.[29] In the present work, we further applied this calculation to a bioblock copolymer system. The detailed amino acid compositions and their properties in A-block, B-block, and H-block are summarized in Table 2, parts a−c, respectively. Note that $M_w(i)$ is the molecular weight mass of the repeating unit of the poly(amino acids). For example,

Table 2. Amino Acids in the A-Block, B-Block, and His-Tag and Their Parameters

amino acid	M_w (g/mol)	number	rotational bonds
	(a) A-Block		
alanine (Ala), A	71.082	7	3
glycine (Gly), G	57.05	5	3
serine (Ser), S	87.078	1	4
threonine (Thr), T	101.10	1	4
A-block totals	970.99[a]	14	44
	(b) B-Block		
glycine (Gly), G	57.05	11	3
leucine (Leu), L	113.16	2	4
glutamine (Gln), Q	128.13	3	6
arginine (Arg), R	156.19	1	8
serine (Ser), S	87.08	3	4
threonine (Thr), T	101.10	1	4
tyrosine (Tyr), Y	163.17	1	4
B-block totals	1919.97[a]	22	87
	(c) His-Tag		
histidine (His), H	137.14	7	5
alanine (Ala), A	71.08	6	3
aspartate (Asp), D	115.09	6	5
glutamate (Glu), E	129.11	2	6
phenylalanine (Phe), F	147.17	1	4
glycine (Gly), G	57.05	4	3
lysine (Lys), K	128.17	3	7
leucine (Leu), L	113.16	2	4
methionine (Met), M	131.20	4	6
proline (Pro), P	97.12	2	4
glutamine (Gln), Q	128.13	1	6
arginine (Arg), R	156.19	2	8
serine (Ser), S	87.08	5	4
threonine (Thr), T	101.10	2	4
valine (Val), V	99.13	1	3
His-tag totals	5217.67[a]	48	225

[a] Sum of: $M_w \times$ number.

we used the molecular weight mass of the repeating unit of poly(glycine), 75.97 − 18.02 = 57.05 g/mol, rather than the molecular weight of glycine, 75.97 g/mol, to calculate the molar mass of the A-block and B-block in the block copolymer. (Note: to calculate the molar mass of A-block and B-block alone, as listed in Table 1, we added 18 g/mol to the calculated molar mass of the A-block and B-block in the block copolymer, which comes from H_2O.) The numbers, N_i, are the total numbers of each type of amino acid existing in the block copolymer, e.g., N_{gly} =5 in the A-block. Knowing the numbers N_i and their corresponding poly(amino acid)s' vibrational heat capacities as a function of temperature (from the ATHAS data bank or estimated), the calculated solid state heat capacity of spider silk block copolymers from 0.1 to 600 K can be constructed by a linear combination of the vibrational heat capacity of each amino acid component. Excellent agreement was found between the measured and calculated values of the heat capacity between 250 K and the glass transition temperature T_g with an error of ±1%. This agreement supports the conclusion that only the vibrational motion of the amino acid components contributes to the heat capacity below T_g and also shows that this can serve as a standard method to predict the solid state heat capacity for other biologically inspired block copolymers.

The heat capacity in the liquid state (viscous liquid, or rubbery state, of the polymer above T_g), $C_p(liquid)$, of spider silk block copolymer above the glass transition can be estimated by considering the contribution comes not only from the vibirational motion, but also from the rotational and translation motion in polymer side chains and backbone. Calculations of the liquid heat capacity for synthetic polymers[41] and a few experimental liquid heat capacity data for biopolymers[25,30] are available but only for a limited temperature range above the glass transition. Empirically, it was found that the liquid state heat capacity is often a linear function of temperature with a smaller slope than that of the solid state heat capacity.[29,41,42] In Table 2, parts a−c, we summarize the number of rotational bonds of the individual amino acids, RB_i, in each block. Knowing the RB_i, the heat capacity increment at the glass transition temperature can be estimated by assuming each rotational bond on average contributes 11 J/(mol K) to the change of heat capacity at the glass transition temperature.[33] Figure 4a−d shows a comparison of the calculated liquid state heat capacity (open circles) of 100% noncrystalline spider silk block copolymers, $C_p(liquid)$ evaluated at T_g, along with the best fit line of the experimental liquid state heat capacity (heavy dashed line). In the case of wholly amorphous copolymers, HAB_3, HBA, and HBA_2, good agreement exist between the best fit line of the experimental values and the calculated value of the heat capacity (Figure 4a−c, open circles) at the glass transition temperature T_g within ±3%. HBA_3 is an exception—the extrapolated line of best fit to the data does not pass through the calculated value of $C_p(liquid)$ because this sample is partially crystalline (crystallinity reduces the heat capacity increment at T_g). The good agreement for amorphous samples supports the conclusion that the vibrational, rotational, and translational motions of the amino acid components all contribute to the liquid state heat capacity above T_g. This agreement also demonstrates the utility of this model to serve as a standard method for predicting the liquid state heat capacity at T_g for other biologically inspired block copolymers.

4.2. Determining the Crystallinity of Spider Silk Block Copolymer by TMDSC. The crystallinity of semicrystalline synthetic polymers is conventionally determined by the enthalpy of fusion from the area of the DSC melting endotherm using $\varphi_C = \Delta H(measured)/\Delta H_f$ where $\Delta H(measured)$ is the heat of fusion obtained from the area of melting peak and ΔH_f is the heat of fusion of 100% crystalline polymer. But, for biopolymers, usually no thermal melting peak can be observed because of their low thermal stability (biopolymers degraded before melting). Thus, usually it is not possible to determine the crystallinity of biopolymers by DSC. However, if we know the theoretical value of the solid state heat capacity and the liquid state heat capacity using the vibrational heat capacity model, we can use an alternate method to calculate the crystallinity by DSC.

The crystallinity of spider silk block copolymers can be determined from their calculated solid state heat capacity, $C_p(vibrational)$, liquid state heat capacity, $C_p(liquid)$, and experimental heat capacity curves, $C_p(experimental)$. By analogy to semicrystalline synthetic polymers,[20,43−45] spider silk block copolymers will be modeled as comprising three phases: (1) the mobile fraction, φ_M, (2) the crystalline β-sheet fraction, φ_C, and (3) the immobilized noncrystalline fraction, φ_{IMM}. The

Table 3. Heat Capacity Increment, Mobile, Rigid, and Crystalline Fractions of Spider Silk Block Copolymers

sample	ΔC_p (kJ/mol K)[a] (±0.02)	ΔC_{p0} (kJ/mol K)[b]	φ_M[c] (±0.02)	φ_{RIGID}[c] (±0.02)	φ_{C_Xray} (±0.03)	φ_{C_FTIR} (±0.03)
B	1.06	1.05	1.0	0	0.03	0
HAB_3	6.39	6.41	1.0	0	0.03	0
HBA	4.31	4.30	1.0	0	0.02	0
HBA_2	4.80	4.84	1.0	0	0.02	0.03
HBA_3	4.05	5.37	0.74	0.26	0.26	0.28
A	0.38	0.53	0.70	0.30	0.31	0.33

[a] Measured data. [b] Calculated heat capacity step at T_g using rotational bonds, RB_i from Table 2. [c] The mobile fraction φ_M and rigid fraction φ_{RIGID} determined by TMDSC using eqs 8 and 9

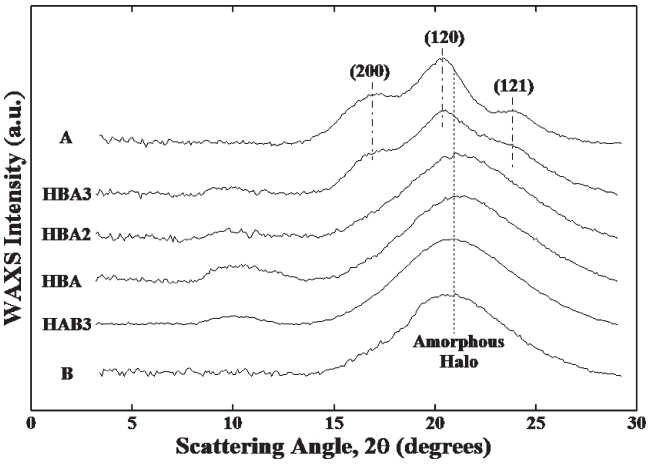

Figure 5. 1-D WAXD patterns for spider silk block copolymers, HBA_3, HBA_2, HBA, and HAB_3. The WAXD patterns for A-block and B-block are also included for reference.

immobilized noncrystalline fraction, φ_{IMM}, is an analogue to the rigid amorphous fraction (RAF) in semicrystalline synthetic polymers, which is amorphous material assumed not to participate in the conventional glass transition process.[46] The β-sheet crystals fraction, φ_C, and the immobilized noncrystalline portions, φ_{IMM}, remained solid-like above the T_g and constitute the rigid fraction, φ_{RIGID}, in spider silk block copolymer. The amorphous region (turns, random coils, α helices, etc.) of spider silk block copolymer constitutes the mobile fraction, φ_M. Therefore, a three-phase model can be use to describe the phase structure of spider silk block copolymer by:

$$\varphi_{RIGID} + \varphi_M = (\varphi_C + \varphi_{IMM}) + \varphi_M = 1 \quad (8)$$

Because the crystalline β-sheet fraction and the immobilized noncrystalline fraction have less molecular mobility, they do not contribute to the glass transition.[46] The heat capacity increment at T_g, ΔC_p, can be used to deduce the mobile fraction, φ_M, from:

$$\varphi_M = \Delta C_p/\Delta C_{p0} = [\Delta C_p/(C_p(liquid) - C_p(vibrational))]|_{T_g} \quad (9)$$

where ΔC_p is the heat capacity increment at T_g; ΔC_{p0} is the calculated heat capacity increment for the 100% noncrystalline spider silk block copolymers, which is the difference between $C_p(vibrational)$ and $C_p(liquid)$ at T_g.

Table 3 lists the measured heat capacity increment, ΔC_p, calculated heat capacity increment for the 100% noncrystalline samples, ΔC_{p0}, and mobile fraction, φ_M, calculated from eq 9. The rigid fraction, φ_{RIGID}, is deduced by subtracting φ_M from unity as discussed in eq 8. The error ranges listed in the table show sample-to-sample variations in the heat capacity as well as experimental error, such as the cell asymmetry within ±0.01 J/g K during measurements. To validate our model, we also used two alternate methods to determine the crystallinity.

WAXD has been used as a conventional method to determine the crystallinity index in both semicrystalline synthetic polymers[26,27,47] and biopolymers[48−50] in Nature. From early studies by Warwicker,[48] β sheet crystal structure of *Nephila* species can be classified into the Warwicker system group 3b using X-ray diffraction analysis. This type of β sheet has a pseudo orthorhombic unit cell[48,51] with dimensions of a = 1.06 nm in the direction of the amino acid side chains, b = 0.944 nm along the direction of the hydrogen bond, and c = 0.695 nm along the main polymer chain.[48,50,51] Figure 5 shows 1-D WAXD patterns of water cast film of the spider silk block copolymers. The X-ray diffraction patterns for A-block and B-block are also included for reference. In Figure 5, three major crystalline peaks were observed for HBA_3 and the A-block at 2θ = 17.09°, 20.54°, and 24.20° corresponding to lattice distances d_{200} (β sheet) = 0.520 nm, d_{120} (β sheet) = 0.433 nm and d_{121} (β sheet) = 0.371 nm, respectively.[48,50] A broad peak of the amorphous halo centered at 2θ = 22.06° was also observed for all samples. Results indicate that a minimum of three A-blocks are required to form β sheet crystalline regions at room temperature in water cast spider silk block copolymer films.

As described in our previous work,[26,27] the crystallinity index can be calculated using the area of crystal peaks and the area of the amorphous halo by fitting the Lorentz-corrected WAXD peak intensity with Gaussian wave functions using a Nelder−Mead simplex direct search routine.[26] The crystalline β sheet fraction gives rise to relatively sharp diffraction peaks, and the amorphous fraction causes a broad scattering halo. The ratio of the area of crystal peaks to the total area gives the crystallinity index, φ_{C_Xray}. Examples of this procedure are shown in Figure 6a,b for HBA_3 (semicrystalline sample) and HAB_3 (nearly amorphous sample), respectively. The amorphous area, Q_a, and the crystalline area, Q_c, were determined by eqs 10a and 10b, and thus the crystallinity index can be determined by eq 10c.

$$Q_a = \int I_a q^2 \, dq \quad (10a)$$

$$Q_c = Q - Q_a = \int I_{corr} q^2 \, dq - \int I_a q^2 \, dq \quad (10b)$$

$$\varphi_{c\_x\,ray} = Q_c/Q \quad (10c)$$

dx.doi.org/10.1021/ma200563t |*Macromolecules* 2011, 44, 5299–5309

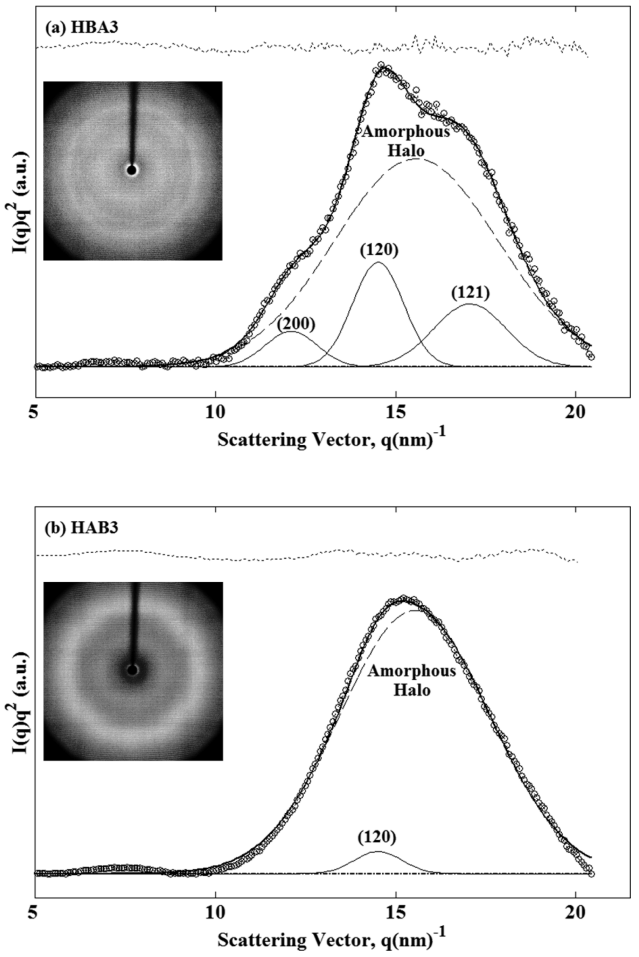

Figure 6. Deconvolution of the Lorentz-corrected WAXD intensity, $I(q)q^2$ vs q, using Gaussian wave functions for (a) HBA_3 (semicrystalline sample) and (b) HAB_3 (nearly amorphous sample). Key: open circles, measured data; heavy line, summation of Gaussian peaks; thin solid lines, individual crystalline Gaussian peaks; dashed lines, amorphous Gaussian peaks; dash-dot lines, baseline; dotted lines, the residual between the fitted curve and measured curve. The inserts shows the 2-D WAXD raw data.

where I_a is the intensity of the amorphous peak, I_{corr} is the scattered intensity after all corrections have been applied and q is the scattering vector. The crystallinity indices, φ_{C_Xray}, are listed in the sixth column of Table 3.

Fourier transform infrared spectroscopy (FTIR) has been used to provide information on the secondary structure of polypeptide and proteins since 1950 by Elliot and Ambrose.[52,53] The amide I (1690−1600 cm^{-1}) and amide II (1575−1480 cm^{-1}) vibrations are sensitive to the secondary structure of the backbone and hardly affected by the nature of the side chain;[54,55] therefore they are most commonly used for secondary structure analysis.[55,56] Water cast films of the spider silk block copolymers on calcium fluoride (CaF_2) substrate were examined. Figure 7 depicts the FTIR absorbance spectra for spider silk block copolymers with the spectra of A-block and B-block as references in amide I and amide II regions. The baseline was fixed for each scan and the air background was also subtracted.

Because the amide I vibration has a more straightforward correlation with secondary structure than the amide II

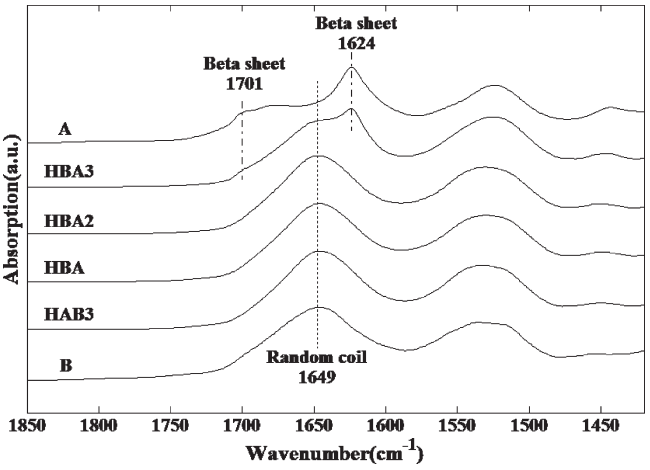

Figure 7. FTIR absorbance spectra for spider silk block copolymers. Prominent bands are marked with vertical lines.

Table 4. Peak Positions and Assignments of the Amide I Region Vibrational Bands of Spider Silk-like Block Copolymer

wavenumber range (cm^{-1})	peak position (cm^{-1}) (±2)	peak assignment	references
1595−1605	1597	(Try) side chains	18, 56−58
1605−1615	1612	(Try) side chains, aggregated strands	18, 56−58
1618−1629	1624	β sheet (strong)	18, 25, 59
1630−1642	1634	random coils, extended chain structures	18, 56, 57, 61−63
1643−1657	1649	random coils	18, 56, 57, 59
1658−1667	1662	α helices	18, 60
1668−1678	1674	turns	25, 55, 60
1679−1685	1684	turns	25, 55, 60
1686−1696	1693	turns	25, 55, 60
1697−1703	1701	high-frequency antiparallel β sheets (weak)	18, 25, 59

vibration,[55,56] we performed Fourier self-deconvolution (FSD) over the amide I peaks on the spectra in Figure 7, using Opus 5.0 software with Lorentzian peak profile (half-bandwidth of 25 cm^{-1} and a noise reduction factor of 0.3). In this process, the broad and indistinct amide I band is transformed to a set of distinct self-deconvoluted bands. The details of this method were discussed in our previous work.[25] After FSD, we fitted the deconvoluted spectra with 10 Gaussian peaks. The peak positions and assignments of the amide I region vibration bands of spider silk block copolymer were determined by reference to the literature, and listed in Table 4. Generally we classify the components between 1620−1630 cm^{-1} to intermolecular β sheets, 1630−1667 cm^{-1} to random coils and α helices, and 1670−1695 cm^{-1} to turns. As shown in Figure 8, the band between 1595 and 1615 cm^{-1} (centered at 1597 and 1612 cm^{-1} in Figure 7 and marked SC in Figure 8) comes from the side chains or aggregated strands;[18,57,58] the band between 1618 and

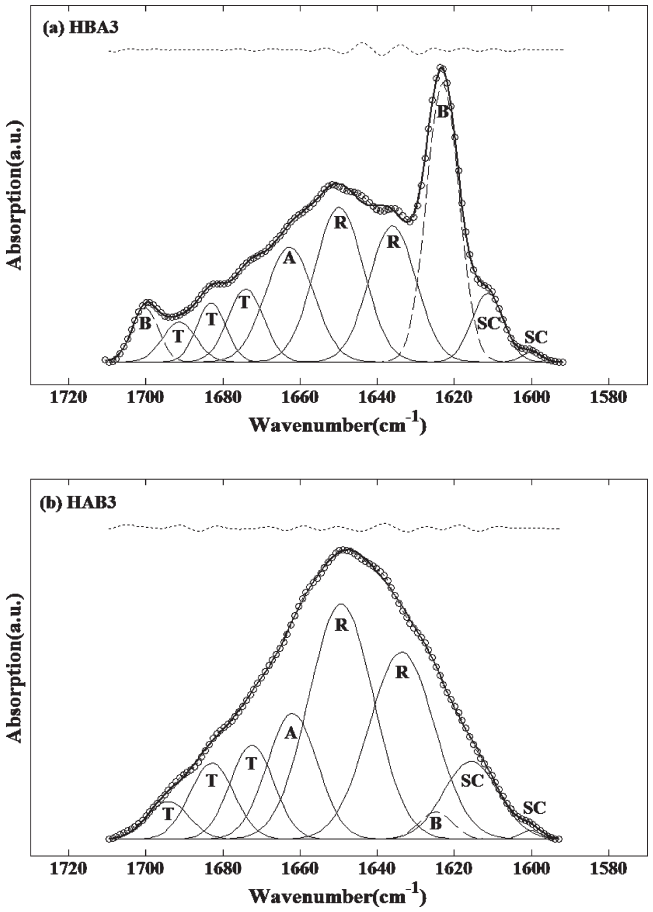

Figure 8. Fourier self-deconvolution of amide I spectra for (a) HBA_3 (semicrystalline sample) and (b) HAB_3 (nearly amorphous sample). Key: open circles, measured data; heavy line, summation of Gaussian peaks; thin solid lines, individual amorphous Gaussian peaks; dashed lines, individual Gaussian peaks from β sheets; dotted lines, the residual between the fitted curve and measured curve. The assignment of amide I bands is taken from the literature[18,25,55−63]and bands are marked as random coil (R), β-sheets (B), α-helices (A), turns (T), and side chains (SC).

1629 cm^{-1} (centered at 1624 cm^{-1} in Figure 7 and marked B in Figure 8) and the band between 1697 and 1703 cm^{-1} (centered at 1701 cm^{-1} in Figure 7, and in also marked B Figure 8) comes from the β sheets;[18,25,59] the band between 1630 and 1642 cm^{-1} and the band between 1643 and 1657 cm^{-1} (centered at 1633 and 1649 cm^{-1} in Figure 7 and marked R in Figure 8) comes from random coils;[18,56,57] the band between 1658 and 1667 cm^{-1} (centered at 1662 cm^{-1} in Figure 7 and marked A in Figure 8) comes from helices structure;[18,60] and the band in the range of 1668−1696 cm-1 (centered at 1674, 1684, and 1693 cm^{-1} in Figure 7 and marked T in Figure 8) usually is contributed by the turns.[25,55,60] Examples of fitted FSD spectra are shown in Figure 8, parts a and b, for HBA_3 (semicrystalline sample) and HAB_3 (nearly amorphous sample), respectively. FTIR results confirm that a minimum of 3 A-blocks are required to form β sheet crystalline regions. It should be pointed out that *B. mori* silk fibroins contain a band centered around 1630 cm^{-1}, which is believed to come from the formation of the intramolecular β-sheets.[25] The band centered at similar wavenumber, 1635−1640 cm^{-1}, was observed in other proteins, such as Elastase and Trypsin, in the less ordered state, which most authors believe comes from the low wavenumber components of a "turns"-like extended chain structure.[61−63] In our spider silk block copolymers, we also observed a peak at 1634 cm^{-1} after FSD. We classified this peak as a random coil contribution, consistent with our WAXD result and the crystallinity determined by heat capacity modeling.

Table 5. Glass Transition Temperature and Theoretical Isoelectric Point (pI) of Spider Silk Block Copolymers

sample	T_g onset (°C) ± 1	T_g inflection (I) (°C) ± 1	T_g end (°C) ± 1	ΔC_{p0} (J/(mol °C)) ± 2	pI
A	131	141	146	538	5.2
B	132	138	142	1063	8.8
BA	117	133	143	1601	8.5
HAB_3	168	174	179	6407	7.1
HBA	171	176	181	4303	6.3
HBA_2	171	178	184	4835	6.3
HBA_3	172	181	190	5367	6.3

The close agreement between the total rigid fraction, φ_{RIGID}, calculated from heat capacity modeling and the crystalline fraction from WAXD and FSD of the infrared spectra, φ_{C_Xray} and φ_{C_FTIR}, suggests that the immobilized noncrystalline fraction, φ_{IMM}, is negligible. This result is similar to what we found in the *B. mori* silk fibroin.[25] The crystal fraction accounts for the rigid fraction almost entirely. Therefore, the two phase model is also a more suitable one for these bioblock copolymers.

4.3. Interaction of Blocks in Spider Silk Block Copolymer. The glass transition is an important intrinsic property in a block copolymer or a binary polymer blend. The T_g value as a function of volume fraction reveals the interaction between different components. Generally, it is believed that a single T_g can be observed for all compositions when components of the block polymers are miscible, while two T_g values can be observed in a compatible system where the components of the block polymers are partially miscible.[64] T_g values for pure components do not change with composition in immiscible polymers.[64] In our spider silk block copolymers, we observed a single step change in heat capacity as spider silk block copolymers undergo their glass transition during heating for all compositions (Figure 4). The data in Figure 4 show His-tag, A-block, and B-block are miscible. The T_g values are determined by the inflection point and are summarized in Table 5.

Several models have been proposed to predict block copolymer and polymer blend glass transition temperatures, such as the Fox equation,[65] Gordon−Taylor equation,[66] and Couchman equations.[67] Although these equations have been successfully applied to certain blends and copolymers, for diblock copolymers and miscible blends, when specific interactions exist between components, these equations do not actually coincide with the experimental T_g.[68] Kwei's equation[69] adds in a term to the Gordon−Taylor equation corresponding to the strength of polymer chain interaction, which may include hydrogen bonding, in the block copolymer[70,71] or blend.[71,72] Therefore, it is the most popular equation applicable for systems with specific interactions:

$$T_g = \frac{(W_1 T_{g1} + W_2 T_{g2})}{(W_1 + kW_2)} + qW_1 W_2 \qquad (11)$$

where W_1 and W_2 are weight fractions of pure components, T_{g1}

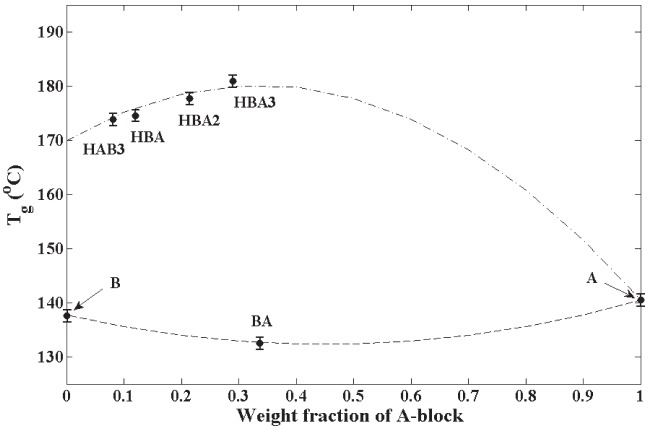

Figure 9. Glass transition temperature vs weight fraction of A-block. Key: filled circles, T_g value for each composition (as marked); dashed line, best fit line of spider silk block copolymer without His-tag using Kwei's eq 11 with $k = 1$ and $q = -27$; dash-dot line, best fit line of spider silk block copolymer with a His-tag using Kwei's eq 11 with $k = 1$ and $q = 90$.

and T_{g2} represent the corresponding glass transition temperatures, and k and q are fitting constants.

The T_g values determined by the inflection point as a function of weight fraction of A-block is plotted in Figure 9. The T_g value of the block copolymer without His-tag (BA) and with His-tag (HAB_3, HBA, HBA_2, and HBA_3) were fitted separately by Kwei's eq 11 and are shown in Figure 9 by dashed line and dash-dot line, respectively. For simplicity, we adopt $k = 1$ in both cases.[70,71,73] For non-His polymer, $q = -27$. For polymers with His-tag, because the His-tag and B have a similar secondary structure, we treated them as one block, which leads to $q = 90$. According to Lin,[74] when $k = 1$, $q < 0$, the enthalpy of mixing must be negative for the two polymers to be compatible, and the overall interaction between the polymers must therefore be attractive. The energy barrier to backbone movement decreases, which leads to a lower T_g. On the other hand, when $k = 1$, $q > 0$, the energy barrier to backbone movement increases, which leads to a higher T_g.[74] Thus, we can conclude that in the dry, condensed state, attractive interaction exists between the A-block and B-block.

To further investigate the origin of the interaction between blocks, the theoretical isoelectric point (pI) of all compositions was calculated by using the Compute pI/M_w tool from Expert Protein Analysis System (ExPASy)[75] based on their amino acid sequences. From the Compute pI/M_w tool, we have PI (A-block) = 5.2, PI (B-block) = 8.8, PI (His-tag) = 6.1 and PI (HB) = 6.3, which means A-block, His-tag and HB-block are slightly negatively charged, and B-block is positively charged in a neutral (pH = 7) environment. This is the reason for the attractive force between A-block and B-block. The PI values of spider silk block copolymers are summarized in the last column of Table 5.

CONCLUSIONS

We have characterized the thermal properties of our newly synthesized family of diblock copolymers inspired by *N. clavipes* major ampulate dragline spider silk, comprising an alanine-rich hydrophobic A-block, a glycine-rich hydrophilic B-block, and a histidine tag, H. The secondary structure and crystal fraction can be controlled by the volume fraction of each block. By WAXD and FTIR studies, we conclude that a minimum of 3 A-blocks is required to form β sheet crystals in the spider silk block copolymer.

In this work, we also successfully predicted the solid state heat capacities of our novel block copolymers based on the vibrational motions of the constituent poly(amino acid)s using heat capacity data from the ATHAS Data Bank. The liquid state heat capacity was estimated by the sum of rotational and translational motions of individual amino acid residues in spider silk block copolymers. Excellent agreement was found between the measured and predicted values of the heat capacity. From our prediction of heat capacity, we provide an alternate method to estimate the crystallinity from DSC for biological polymers, whose melting peak is usually unobservable because of relatively low thermal stability. Our result is confirmed by both WAXD and FTIR. The close agreement between the total rigid fraction, calculated from heat capacity modeling, and the crystalline fraction, from WAXD and FSD of the infrared spectra, suggests that the immobilized noncrystalline fraction is negligible. A two phase model is therefore more suitable for the bioblock copolymers. Interaction of blocks in spider silk block copolymer was studied by Kwei's equation applied to the glass transition temperatures of spider silk block copolymer and results indicate that attractive interaction exists between the A-block and B-block.

AUTHOR INFORMATION

Corresponding Author

*E-mail: peggy.cebe@tufts.edu.

ACKNOWLEDGMENT

The authors thank the National Science Foundation, Division of Chemical, Bioengineering, Environmental, and Transport Systems, for support of this research through Grant CBET-0828028 and the MRI Program under DMR-0520655 for thermal analysis instrumentation. The author thanks Ms. Q. Ma for the help with Matlab software.

REFERENCES

(1) McGrath, K.; Kaplan, D., *Protein-based materials*. Birkhäuser: Boston, MA, 1997; pp 104−105.

(2) Gosline, J. M.; Guerette, P. A.; Ortlepp, C. S.; Savage, K. N. *J. Exp. Biol.* **1999**, *202* (23), 3295–3303.

(3) Sponner, A.; Schlott, B.; Vollrath, F.; Unger, E.; Grosse, F.; Weisshart, K. *Biochemistry* **2005**, *44* (12), 4727–4736.

(4) Kluge, J. A.; Rabotyagova, U.; Leisk, G. G.; Kaplan, D. L. *Trends Biotechnol.* **2008**, *26* (5), 244–251.

(5) Cunniff, P. M.; Fossey, S. A.; Auerbach, M. A.; Song, J. W. *Silk Polym.—Mater. Sci. Biotechnol.* **1994**, *544*, 234–251.

(6) Gosline, J. M.; Demont, M. E.; Denny, M. W. *Endeavour* **1986**, *10* (1), 37–43.

(7) Foelix, R. F., *Biology of spiders*, 2nd ed.; Oxford University Press: New York, 1996; p 330.

(8) Vendrely, C.; Scheibel, T. *Macromol. Biosci.* **2007**, *7* (4), 401–409.

(9) Sofia, S.; McCarthy, M. B.; Gronowicz, G.; Kaplan, D. L. *J. Biomed. Mater. Res.* **2001**, *54* (1), 139–148.

(10) Rising, A.; Nimmervoll, H.; Grip, S.; Fernandez-Arias, A.; Storckenfeldt, E.; Knight, D. P.; Vollrath, F.; Engstrom, W. *Zool. Sci.* **2005**, *22* (3), 273–281.

(11) Hayashi, C. Y.; Shipley, N. H.; Lewis, R. V. *Int. J. Biol. Macromol.* **1999**, *24* (2−3), 271–275.

(12) Li, S. C.; Goto, N. K.; Williams, K. A.; Deber, C. M. *Proc. Natl. Acad. Sci. U.S.A.* **1996**, *93* (13), 6676–6681.

(13) Liu, Y.; Sponner, A.; Porter, D.; Vollrath, F. *Biomacromolecules* **2008**, *9* (1), 116–121.
(14) Hu, X.; Vasanthavada, K.; Kohler, K.; McNary, S.; Moore, A. M. F.; Vierra, C. A. *Cell. Mol. Life Sci.* **2006**, *63* (17), 1986–1999.
(15) Simmons, A.; Ray, E.; Jelinski, L. W. *Macromolecules* **1994**, *27* (18), 5235–5237.
(16) Gosline, J.; Lillie, M.; Carrington, E.; Guerette, P.; Ortlepp, C.; Savage, K. *Philos. Trans. R. Soc., London, Ser. B: Biol. Sci.* **2002**, *357* (1418), 121–132.
(17) Hayashi, C. Y.; Lewis, R. V. *J. Mol. Biol.* **1998**, *275* (5), 773–784.
(18) Rabotyagova, O. S.; Cebe, P.; Kaplan, D. L. *Biomacromolecules* **2009**, *10* (2), 229–236.
(19) Krishnaji, S. T.; Huang, W. W.; Rabotyagova, O.; Kharlampieva, E.; Choi, I.; Tsukruk, V. V.; Naik, R.; Cebe, P.; Kaplan, D. L. *Langmuir* **2011**, *27* (3), 1000–1008.
(20) Xu, H.; Cebe, P. *Macromolecules* **2004**, *37* (8), 2797–2806.
(21) Boller, A.; Okazaki, I.; Ishikiriyama, K.; Zhang, G.; Wunderlich, B. *J. Therm. Anal.* **1997**, *49* (2), 1081–1088.
(22) Ishikiriyama, K.; Wunderlich, B. *J. Therm. Anal.* **1997**, *50* (3), 337–346.
(23) Press, W. H., *Numerical recipes: the art of scientific computing*, 3rd ed.; Cambridge University Press: Cambridge, U.K., 2007; pp 607−609.
(24) Xu, S. X.; Li, Y.; Feng, Y. P. *Thermochim. Acta* **2000**, *343* (1−2), 81–88.
(25) Hu, X.; Kaplan, D.; Cebe, P. *Macromolecules* **2006**, *39* (18), 6161–6170.
(26) Buckley, J.; Cebe, P.; Cherdack, D.; Crawford, J.; Ince, B. S.; Jenkins, M.; Pan, J. J.; Reveley, M.; Washington, N.; Wolchover, N. *Polymer* **2006**, *47* (7), 2411–2422.
(27) Huang, W. W.; Edenzon, K.; Fernandez, L.; Razmpour, S.; Woodburn, J.; Cebe, P. *J. Appl. Polym. Sci.* **2010**, *115* (6), 3238–3248.
(28) Wunderlich, B. *Thermochim. Acta* **1997**, *300* (1−2), 43–65.
(29) Pyda, M.; Hu, X.; Cebe, P. *Macromolecules* **2008**, *41* (13), 4786–4793.
(30) Hu, X.; Kaplan, D.; Cebe, P. *Thermochim. Acta* **2007**, *461* (1−2), 137–144.
(31) Wunderlich, B. *Pure Appl. Chem.* **1995**, *67* (6), 1019–1026.
(32) Pyda, M. Private communication, 2007.
(33) Pyda, M. The Advanced Thermal Analysis System (ATHAS) Data Bank, http://athas.prz.rzeszow.pl/Default.aspx?op=db.
(34) Minakov, A. A.; Mordvintsev, D. A.; Schick, C. *Polymer* **2004**, *45* (11), 3755–3763.
(35) Wunderlich, B., *Thermal analysis of polymeric materials*. Springer: Berlin, 2005; p xvi, 894 p.
(36) Hodge, R. M.; Bastow, T. J.; Edward, G. H.; Simon, G. P.; Hill, A. J. *Macromolecules* **1996**, *29* (25), 8137–8143.
(37) Kim, Y. S.; Dong, L. M.; Hickner, M. A.; Glass, T. E.; Webb, V.; McGrath, J. E. *Macromolecules* **2003**, *36* (17), 6281–6285.
(38) Lee, K. Y.; Ha, W. S. *Polymer* **1999**, *40* (14), 4131–4134.
(39) Roles, K. A.; Wunderlich, B. *Biopolymers* **1991**, *31* (5), 477–487.
(40) Roles, K. A.; Xenopoulos, A.; Wunderlich, B. *Biopolymers* **1993**, *33* (5), 753–768.
(41) Pyda, M. *J. Polym. Sci., Part B: Polym. Phys.* **2001**, *39* (23), 3038–3054.
(42) Pyda, M.; Wunderlich, B. *Macromolecules* **2005**, *38* (25), 10472–10479.
(43) Chen, H. P.; Cebe, P. *Macromolecules* **2009**, *42* (1), 288–292.
(44) Pak, J.; Pyda, M.; Wunderlich, B. *Macromolecules* **2003**, *36* (2), 495–499.
(45) Schick, C.; Wurm, A.; Mohammed, A. *Thermochim. Acta* **2003**, *396* (1−2), 119–132.
(46) Menczel, J.; Wunderlich, B. *J. Polym. Sci., Part C: Polym. Lett.* **1981**, *19* (5), 261–264.
(47) Decher, G. *Science* **1997**, *277* (5330), 1232–1237.
(48) Warwicker, J. O. *J. Mol. Biol.* **1960**, *2* (6), 350–&.
(49) Krejchi, M. T.; Cooper, S. J.; Deguchi, Y.; Atkins, E. D. T.; Fournier, M. J.; Mason, T. L.; Tirrell, D. A. *Macromolecules* **1997**, *30* (17), 5012–5024.
(50) Glisovic, A.; Vehoff, T.; Davies, R. J.; Salditt, T. *Macromolecules* **2008**, *41* (2), 390–398.
(51) Marsh, R. E.; Corey, R. B.; Pauling, L. *Biochim. Biophys. Acta* **1955**, *16* (1), 1–34.
(52) Ambrose, E. J.; Elliott, A. *Proc. R. Soc. London, Ser. A: Math. Phys. Sci.* **1951**, *206* (1085), 206–219.
(53) Ambrose, E. J.; Elliott, A. *Proc. R. Soc. London, Ser. A: Math. Phys. Sci.* **1951**, *208* (1092), 75–90.
(54) Barth, A. *Prog. Biophys. Mol. Biol.* **2000**, *74* (3−5), 141–173.
(55) Barth, A. *Biochim. Biophys. Acta-Bioenergetics* **2007**, *1767* (9), 1073–1101.
(56) Barth, A.; Zscherp, C. *Q. Rev. Biophys.* **2002**, *35* (4), 369–430.
(57) Jackson, M.; Mantsch, H. H. *Crit. Rev. Biochem. Mol. Biol.* **1995**, *30* (2), 95–120.
(58) Jung, C. *J. Mol. Recognition* **2000**, *13* (6), 325–351.
(59) Chen, X.; Knight, D. P.; Shao, Z. Z.; Vollrath, F. *Biochemistry* **2002**, *41* (50), 14944–14950.
(60) Dicko, C.; Knight, D.; Kenney, J. M.; Vollrath, F. *Biomacromolecules* **2004**, *5* (6), 2105–2115.
(61) Byler, D. M.; Susi, H. *Biopolymers* **1986**, *25* (3), 469–487.
(62) Susi, H.; Byler, D. M. *Methods Enzymol.* **1986**, *130*, 290–311.
(63) Arrondo, J. L. R.; Muga, A.; Castresana, J.; Goni, F. M. *Prog. Biophys. Mol. Biol.* **1993**, *59* (1), 23–56.
(64) Brostow, W.; Chiu, R.; Kalogeras, I. M.; Vassilikou-Dova, A. *Mater. Lett.* **2008**, *62* (17−18), 3152–3155.
(65) Fox, T. G. *Bull. Am. Phys. Soc.* **1956**, *1*, 123.
(66) Gordon, M.; Taylor, J. S. *J. Appl. Chem.* **1952**, *2* (9), 493–500.
(67) Couchman, P. R. *Macromolecules* **1991**, *24* (21), 5772–5774.
(68) Widmaier, J. M.; Meyer, G. C. *J. Therm. Anal.* **1982**, *23* (1−2), 193–199.
(69) Kwei, T. K. *J. Polym. Sci., Part C: Polym. Lett.* **1984**, *22* (6), 307–313.
(70) Kuo, S. W.; Tung, P. H.; Chang, F. C. *Macromolecules* **2006**, *39* (26), 9388–9395.
(71) Chen, W. C.; Kuo, S. W.; Jeng, U. S.; Chang, F. C. *Macromolecules* **2008**, *41* (4), 1401–1410.
(72) Chen, H. P.; Pyda, M.; Cebe, P. *Thermochim. Acta* **2009**, *492* (1−2), 61–66.
(73) Kuo, S. W.; Liu, W. P.; Chang, F. C. *Macromolecules* **2003**, *36* (14), 5165–5173.
(74) Lin, A. A.; Kwei, T. K.; Reiser, A. *Macromolecules* **1989**, *22* (10), 4112–4119.
(75) Expert Protein Analysis System (ExPASy) proteomics server, http://expasy.org/, **02/2011**.